DESY 98-113
DAMTP-1998-113

DESY 98-113 ISSN 0418-9833
DAMTP-1998-113
August 1998

hep-ph/9808454 28 Aug 1998

Inclusive and Diffractive Structure Functions at Small x

W. Buchmüller, T. Gehrmann
Deutsches Elektronen-Synchrotron DESY, 22603 Hamburg, Germany
and
A. Hebecker
D.A.M.T.P., Cambridge University, Cambridge CB3 9EW, England

Abstract

In the semiclassical approach, inclusive and diffractive quark and gluon distributions are expressed in terms of correlation functions of Wilson loops. Each Wilson loop integrates the colour field strength in the area between the trajectories of two fast partons penetrating the proton. We introduce a specific model for averaging over the relevant colour field configurations. Within this model, all parton distributions at some low scale Q_0^2 are given in terms of three parameters. Inclusive and diffractive structure functions at higher values of Q^2 are determined in a leading-order QCD analysis. In both cases, the evolution is driven by a large gluon distribution. A satisfactory description of the structure functions $F_2(x,Q^2)$ and $F_2^{D(3)}(\xi,\beta,Q^2)$ is obtained. The observed rise of $F_2^{D(3)}$ with ξ is parametrized by a non-perturbative logarithmic energy dependence, compatible with unitarity. In our analysis, the observed rise of F_2 at small x is largely due to the same effect.

1 Introduction

Recently, precise measurements of inclusive [1] and diffractive [2] structure functions at small x have become available. Numerical analyses, based on different theoretical approaches, have been performed by many authors (see e.g. [3–6]).

In the present paper, a joint analysis of diffractive and inclusive structure functions based on the semiclassical calculations of [7,8] is performed. The idea of a close similarity between diffractive and non-diffractive processes in deep inelastic scattering (DIS) lies at the heart of the semiclassical approach. In both cases, a partonic fluctuation of the incoming virtual photon scatters off a superposition of target colour fields. If the scattered partons emerge in an overall colour singlet configuration, a diffractive final state results.

Comparing the semiclassical description of structure functions with parton model expressions, we define inclusive and diffractive [9] parton distributions in the semiclassical approach. Higher order contributions in the semiclassical calculation exactly reproduce the leading logarithmic corrections to the parton model, showing the consistency of both approaches. The semiclassical method is therefore used at some low scale to derive initial distributions. Starting from these distributions, a leading-order DGLAP analysis [10] of experimental data is performed.

The calculation of the above initial distributions involves averaging over all relevant colour field configurations. To perform this averaging, a simple non-perturbative model, valid in the case of large hadronic targets [11], is used. It is based on the observation that, for extended target colour fields, the transverse size of partonic fluctuations of the photon remains small [12].

The energy dependence arising from the large-momentum cutoff applied in the process of colour field averaging can not be calculated from first principles. It is described by a $\ln^2 x$ ansatz, consistent with unitarity. In the semiclassical approach, this energy dependence is expected to be universal for both the inclusive and diffractive structure functions [13].

Overall, a satisfactory description of inclusive and diffractive small-x structure functions, based on a minimal number of assumptions and only four fitted parameters, is achieved. In our opinion, this lends support to the idea of a close similarity between the mechanisms of inclusive and diffractive scattering and its implementation in the semiclassical approach.

The paper is organized as follows. In Sections 2 and 3, semiclassical formulae for inclusive and diffractive parton distributions are given, and the underlying physical picture is discussed. Section 4 deals with our model for the colour field averaging that is responsible for the input distributions. The leading-order DGLAP analysis and the comparison with experimental data are the subject of Sect. 5, followed by conclusions in Sect. 6. Appendix A contains some additional formulae relevant for the calculation of the diffractive parton distribution functions. Finally, we illustrate in Appendix B how the diffractive parton distributions of a small colour dipole, calculated in [14], can be obtained using the semiclassical method.

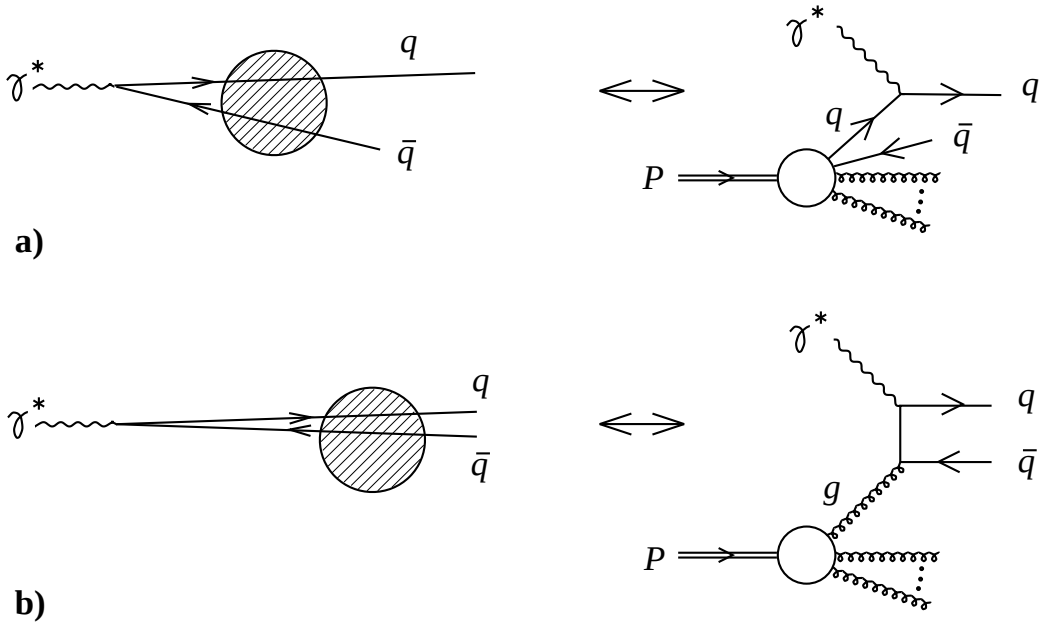

Figure 1: Inclusive DIS in the proton rest frame (left) and the Breit frame (right); asymmetric fluctuations correspond to quark scattering (a), symmetric fluctuations to boson-gluon fusion (b).

2 Inclusive structure functions

Small-x DIS can be conveniently discussed in terms of the $q\bar{q}$ wave function of the virtual photon (see e.g. [3]). In the semiclassical approach, the corresponding $q\bar{q}$ states scatter off a 'soft' target colour field (cf. the l.h. side of Fig. 1). As $x \to 0$, the resulting inclusive structure function $F_T(x,Q^2)$ approaches a constant [7],

$$F_T(x,Q^2) = \frac{2Q^2e_q^2}{(2\pi)^4}\int_0^1 d\alpha(\alpha^2+(1-\alpha)^2)N^2\int_{y_\perp}K_1(yN)^2\int_{x_\perp}\mathrm{tr}\left(W^{\mathcal{F}}_{x_\perp}(y_\perp)W^{\mathcal{F}\dagger}_{x_\perp}(y_\perp)\right) + \mathcal{O}(x)\,. \quad (1)$$

The light-like paths of quark and antiquark penetrate the colour field of the proton at transverse positions $x_\perp$ and $x_\perp + y_\perp$ picking up non-Abelian phase factors $U^{\mathcal{F}}(x_\perp)$ and $U^{\mathcal{F}\dagger}(x_\perp+y_\perp)$ (where $\mathcal{F}$ stands for the fundamental representation). The function

$$W^{\mathcal{F}}_{x_\perp}(y_\perp) = U^{\mathcal{F}}(x_\perp)U^{\mathcal{F}\dagger}(x_\perp+y_\perp) - 1 \quad (2)$$

is essentially a closed Wilson loop through the corresponding section of the proton, which measures an integral of the proton colour field strength. Furthermore, α is the fraction of the photon momentum carried by the quark, $N^2 = \alpha(1-\alpha)Q^2$, $y = |y_\perp|$ and e_q is the quark charge.

To map this calculation onto the conventional parton model framework, extract the leading-twist contribution from Eq. (1) and identify it with $F_T(x,Q^2) = 2e_q^2 xq(x,Q^2)$.

The resulting quark distribution reads

$$xq(x,Q^2) = \frac{2}{(2\pi)^4}\int_0^{\mu^2} N^2\,dN^2 \int_{y_\perp} K_1(yN)^2 \int_{x_\perp} \mathrm{tr}\left(W^{\mathcal{F}}_{x_\perp}(y_\perp)W^{\mathcal{F}\dagger}_{x_\perp}(y_\perp)\right) + \frac{2}{3(2\pi)^3}\left(\ln\frac{Q^2}{\mu^2}-1\right)\int_{x_\perp}\mathrm{tr}\left(\partial_{y_\perp}W^{\mathcal{F}}_{x_\perp}(0)\partial_{y_\perp}W^{\mathcal{F}\dagger}_{x_\perp}(0)\right)\ . \qquad (3)$$

Note that this expression is independent of μ^2, which has only been introduced to separate the logarithmic Q^2 dependence explicitly. We have assumed that the hadronic structure, encoded in the y^2 dependence of $WW^\dagger$, is dominated by the soft scale Λ^2, which satisfies $\Lambda^2 \ll \mu^2 \ll Q^2$.

The corresponding gluon distribution at small x is most easily calculated as

$$xg(x,Q^2) = \frac{3\pi}{\alpha_s e_q^2}\cdot\frac{\partial F_T(x,Q^2)}{\partial \ln Q^2} = \frac{1}{2\pi^2\alpha_s}\int_{x_\perp}\mathrm{tr}\left(\partial_{y_\perp}W^{\mathcal{F}}_{x_\perp}(0)\partial_{y_\perp}W^{\mathcal{F}\dagger}_{x_\perp}(0)\right)\ . \qquad (4)$$

Equations (3) and (4) provide the basis for our analysis of inclusive DIS. Note that the semiclassical approach predicts $g(x,Q^2)\sim 1/x$, which is expected for a classical bremsstrahlung spectrum of gluons.

To gain more physical insight into the correspondence of the semiclassical and the parton model approach, return to our starting point, Eq. (1). It is instructive to view F_T as a sum of two terms: F_T^{asym}, the contribution of asymmetric configurations where quark or antiquark are slow, $\alpha < \mu^2/Q^2$ or $1-\alpha < \mu^2/Q^2$ (Fig. 1a), and F_T^{sym}, the contribution of symmetric configurations where both quark and antiquark are fast, $\alpha, 1-\alpha > \mu^2/Q^2$ (Fig. 1b). In an infinite momentum frame of the proton, the asymmetric and symmetric contribution to F_T correspond to photon-quark scattering and photon-gluon fusion respectively.

The symmetric part is dominated by small $q\bar{q}$ pairs, i.e., by the short distance contribution to the Wilson-loop trace,

$$\int_{x_\perp}\mathrm{tr}\left(W^{\mathcal{F}}_{x_\perp}(y_\perp)W^{\mathcal{F}\dagger}_{x_\perp}(y_\perp)\right) = \frac{1}{2}y^2\int_{x_\perp}\mathrm{tr}\left(\partial_{y_\perp}W^{\mathcal{F}}_{x_\perp}(0)\partial_{y_\perp}W^{\mathcal{F}\dagger}_{x_\perp}(0)\right)+\mathcal{O}(y^4)\ . \qquad (5)$$

The corresponding contribution to the structure function is related to the second term on the r.h. side of Eq. (3), which generates the gluon distribution, Eq. (4). It was evaluated in [7] at leading order in Λ^2/μ^2 and μ^2/Q^2,

$$F_T^{sym}(0,Q^2) = \frac{e_q^2}{2\pi^3}\int_0^1 dz\,P_{qg}(z)\left(\ln\frac{Q^2}{\mu^2}-1\right)\int_{x_\perp}\mathrm{tr}\left(\partial_{y_\perp}W^{\mathcal{F}}_{x_\perp}(0)\partial_{y_\perp}W^{\mathcal{F}\dagger}_{x_\perp}(0)\right)\ . \qquad (6)$$

Here $P_{qg}(z)$ is the conventional gluon-quark splitting function.

The other splitting functions appear if α_s corrections to F_T and F_L, associated with higher Fock states of the virtual photon, are considered in the semiclassical approach. For example, the $q\bar{q}g$ parton configuration involves, in the case where one of the quarks carries a small fraction of the photon momentum, a $\ln Q^2$ term associated with $P_{qq}(z)$.

The splitting function $P_{gg}(z)$ is most easily derived by considering an incoming virtual scalar which couples directly to the gluonic action term $F_{\mu\nu}F^{\mu\nu}$. Its lowest order Fock state consists of two gluons. We have checked explicitly that the semiclassical calculation of the corresponding high energy scattering process yields the usual gluon-gluon splitting function.

Having shown that the leading logarithmic QCD corrections to the semiclassical approach exactly reproduce the well-known DGLAP splitting functions [10], we do not pursue the calculation of higher order α_s contributions along the lines discussed above. Instead, the large logarithms $\ln(Q^2/\mu^2)$ are resummed in the conventional way, by means of the renormalization group. To this end, the parton distributions $q(x,Q^2)$ and $g(x,Q^2)$ are evaluated using DGLAP evolution equations, with the input distributions $q(x,Q_0^2)$ and $g(x,Q_0^2)$ given by Eqs. (3) and (4). Here Q_0^2 is some small scale where logarithmic corrections are not yet important. The parton model description of the structure function at leading order includes only photon-quark scattering. The leading logarithmic term from the photon-gluon fusion process appears now as part of the resummed quark distribution.

So far, we have considered electroproduction off a fixed 'soft' colour field. As a consequence, the unevolved structure function $F_T(x,Q_0^2)$ approaches a constant value as $x \to 0$. However, a proper treatment of the target requires the integration over all relevant colour field configurations.

The qualitative features of the field averaging procedure are most conveniently discussed for the simple case of $q\bar{q}$ pair production in the proton rest frame. Consider the corresponding amplitude in a 'mixed' representation, $< q\bar{q}\,A\,|\,\gamma^* p >$, where the final state consists of the outgoing $q\bar{q}$ pair and a colour field configuration A. We neglect any time evolution of the field between the actual scattering process and the moment at which the final state field configuration A is defined. The squared amplitude, summed over all fields A and normalized to the total space-time volume, reads

$$\frac{1}{VT}\int_A |< q\bar{q}\,A\,|\,\gamma^* p >|^2 = 4\pi m_p \delta(k_q^0 + k_{\bar{q}}^0 - q^0)\int_{A_{loc}} \Big|\,\Phi_p[A_{loc}]\,F[A_{loc}]\,\Big|^2 . \qquad (7)$$

Here Φ_p is the proton wave functional, F is defined by the amplitude for the scattering off a fixed field A,

$$< q\bar{q}\,|\,\gamma^*\,>_A = 2\pi\delta(k_q^0 + k_{\bar{q}}^0 - q^0)\,F[A]\,, \qquad (8)$$

m_p is the proton mass, and q, k_q, $k_{\bar{q}}$ are the momenta of the incoming photon and the outgoing quark and antiquark respectively. The index '*loc*' symbolizes that, on the r.h. side of Eq. (7), the integration is restricted to fields localized at, say, $\vec{x} = 0$. This can be justified using translation covariance of the proton wave functional and of the matrix element $< q\bar{q}\,|\,\gamma^*\,>_A$ (cf. Sect. 2 of [7]).

When writing $W_{x_\perp}^{\mathcal{F}}(y_\perp)$ we have, until now, always assumed the functional dependence on the classical colour field configuration A_{cl} to be implicit, so that one should really read $W_{x_\perp}^{\mathcal{F}}(y_\perp)[A_{cl}]$. As can be seen from Eq. (7), the full inclusive parton distribu-

tions are obtained from the previous formulae by the substitution

$$\mathrm{tr}\Big(W^{\mathcal{F}}_{x_\perp}(y_\perp)[A_{cl}]\,W^{\mathcal{F}\dagger}_{x_\perp}(y_\perp)[A_{cl}]\Big) \to \int_{A_{loc}} \Big|\,\Phi_p[A_{loc}]\,\Big|^2\ \mathrm{tr}\Big(W^{\mathcal{F}}_{x_\perp}(y_\perp)[A_{loc}]\,W^{\mathcal{F}\dagger}_{x_\perp}(y_\perp)[A_{loc}]\Big)\,. \tag{9}$$

The same applies to the diffractive distributions of the next section. An explicit model for the field average will be described in Sect. 4.

Decomposing the field A_{loc} in Eq. (7) into its Fourier modes $\tilde{A}_{loc}(\vec{k})$, the path integral can be written as

$$\int_{A_{loc}} = \prod_{|\vec{k}|\ll|\vec{q}|} \int d\tilde{A}_{loc}(\vec{k})\,, \tag{10}$$

where the cutoff $|\vec{q}|$ is required to ensure that the basic precondition for the semiclassical treatment, the softness of the target colour field with respect to the momenta of the fast particles, is respected. This cutoff induces a non-trivial energy dependence of the squared amplitude in Eq. (7).

We are not able to derive the explicit form of that energy dependence from first principles. Nevertheless, based on the above qualitative discussion, we ascribe a soft, non-perturbative energy growth to our input parton distributions used in the numerical analysis of Sect. 5.

3 Diffractive structure functions

The diffractive cross sections obtained in the semiclassical approach [7] can be expressed as convolution of the ordinary partonic cross sections and diffractive parton distributions, calculated in [8]. The $q\bar{q}$ and $q\bar{q}g$ configurations then yield

$$\begin{aligned}\frac{d\sigma_{T,L}}{d\xi} &= \int_x^\xi dy \Bigg\{ \Big(\hat{\sigma}_{T,L}(y)^{\gamma^* q\to q} + \hat{\sigma}_{T,L}(y)^{\gamma^* q\to qg}\Big)\ \frac{dq(x/y,\xi)}{d\xi} \\ &\qquad + \hat{\sigma}_{T,L}(y)^{\gamma^* g\to q\bar{q}}\ \frac{dg(x/y,\xi)}{d\xi}\Bigg\}\,. \end{aligned} \tag{11}$$

Here ξ is related to the diffractive mass M by $\xi = x_{I\!P} = x/\beta$ and $\beta = Q^2/(Q^2+M^2)$. The corresponding structure functions read

$$\begin{aligned} F_T^D(\xi,\beta,Q^2) &= 2e_q^2 x \int_\beta^1 \frac{db}{b}\Bigg\{ \left(\delta(1-z) + \frac{\alpha_s}{2\pi}\left(P_{qq}(z)\ln\frac{Q^2}{\mu^2} + \ldots\right)\right)\frac{dq(b,\xi)}{d\xi} \\ &\qquad + \frac{\alpha_s}{2\pi}\left(P_{qg}(z)\ln\frac{Q^2}{\mu^2} + \ldots\right)\frac{dg(b,\xi)}{d\xi}\Bigg\}\,, \end{aligned} \tag{12}$$

$$F_L^D(\xi,\beta,Q^2) = 2e_q^2 x\frac{\alpha_s}{2\pi}\int_\beta^1 \frac{db}{b}\left\{2C_F z\frac{dq(b,\xi)}{d\xi} + 4T_F z(1-z)\frac{dg(b,\xi)}{d\xi}\right\}\,, \tag{13}$$

where $z = \beta/b$, and C_F and T_F are the usual colour factors. The physical interpretation of the diffractive parton distributions in the Breit frame is analogous to the interpretation

of the inclusive distributions. The function $df(b,\xi)/d\xi$ (where $f = q, g$) is a conditional probability distribution. It describes the probability of finding a parton f, carrying a fraction ξb of the proton momentum, inside a colour-neutral cluster of partons that carries in total a fraction ξ of the proton momentum.

From Eqs. (12) and (13), it is obvious that the diffractive structure functions satisfy the ordinary DGLAP evolution equations (cf. the more general discussion of [15]). The perturbative evolution takes place in the variables β and Q^2; ξ acts merely as a parameter. The physical reason for this is intuitively clear: for an arbitrary DIS event the invariant hadronic mass is W, and the quark which couples to the virtual photon can be radiated by a parton whose fraction of the proton momentum varies from 1 to $x = Q^2/(Q^2+W^2)$. In a diffractive event, a colour-neutral cluster of 'wee partons' is stripped off the proton. The invariant mass of this cluster and the virtual photon is M. Hence, W is replaced by M, and the quark which couples to the photon can be radiated by a parton whose fraction of the cluster momentum varies from 1 to $\beta = Q^2/(Q^2 + M^2)$.

The separation of the colour-neutral cluster of 'wee partons' is non-perturbative and independent of the perturbative evolution. It is, however, incorrect to visualize a two-step process where the colour-neutral cluster is first emitted by the proton and then probed by the virtual photon. If this was the case, the two-gluon or two-quark cluster relevant in our calculation (cf. the r.h. side of Fig. 2) would necessarily lead to parton distributions symmetric in β and $1-\beta$. A counter example to this is provided by the model distributions derived in Sect. 4.

The diffractive quark and gluon distributions have been determined in [8]. In terms of Wilson loops in coordinate space, the quark distribution can be expressed as follows (cf. Appendix A),

$$\begin{aligned}\frac{dq(b,\xi)}{d\xi} &= \frac{2b}{\xi^2(1-b)^3}\int\frac{d^2k'_\perp\,k'^4}{(2\pi)^6 N_c}\int_{y_\perp,y'_\perp} e^{ik'_\perp(y_\perp-y'_\perp)}\,\frac{y_\perp y'_\perp}{y\,y'} \\ &\quad\times K_1(yN)K_1(y'N)\int_{x_\perp}\mathrm{tr}W^{\mathcal{F}}_{x_\perp}(y_\perp)\mathrm{tr}W^{\mathcal{F}\dagger}_{x_\perp}(y'_\perp)\;, \end{aligned} \tag{14}$$

where N_c is the number of colours and

$$N^2 = k'^2\frac{b}{1-b}\;. \tag{15}$$

The corresponding expression for the diffractive gluon distribution is very similar. Because of the different colour and spin of the gluon, the Wilson loop is now in the adjoint representation, the tensor structure is different and the modified Bessel function K_2 appears[1],

$$\begin{aligned}\frac{dg(b,\xi)}{d\xi} &= \frac{b}{\xi^2(1-b)^3}\int\frac{d^2k'_\perp\,k'^4}{(2\pi)^6 N_c^2}\int_{y_\perp,y'_\perp} e^{ik'_\perp(y_\perp-y'_\perp)}\,t_{ij}(y_\perp)t_{ij}(y'_\perp) \\ &\quad\times K_2(yN)K_2(y'N)\int_{x_\perp}\mathrm{tr}W^{\mathcal{A}}_{x_\perp}(y_\perp)\mathrm{tr}W^{\mathcal{A}\dagger}_{x_\perp}(y'_\perp)\;, \end{aligned} \tag{16}$$

[1]To simplify the colour algebra of Sect. 4, we use the large N_c limit throughout this paper, with the exception of the standard DGLAP evolution in Sect. 5.

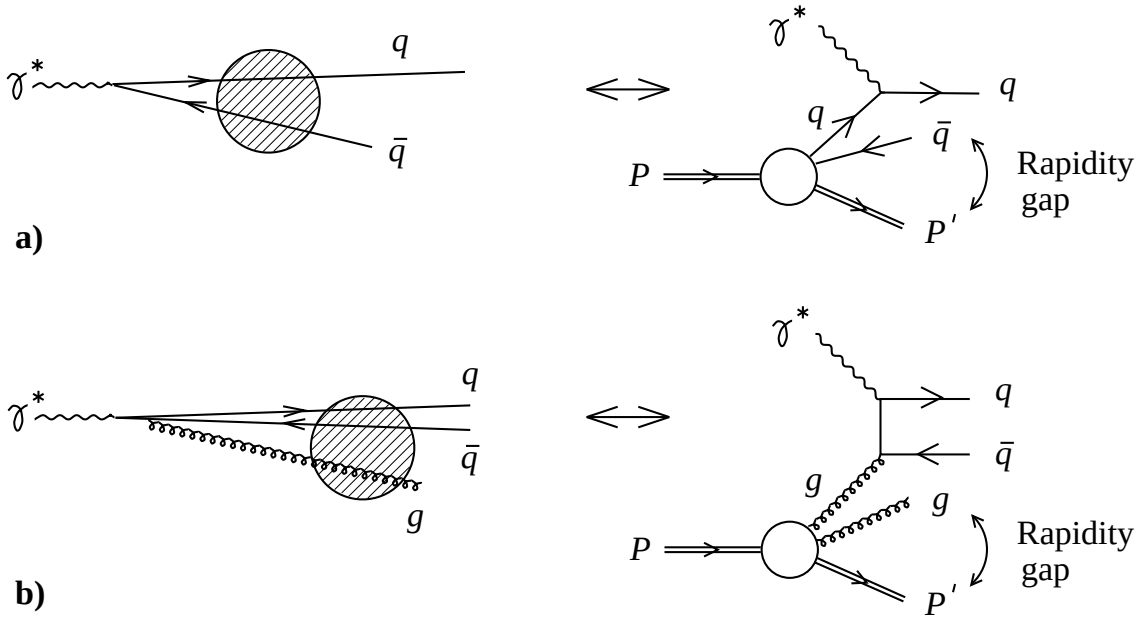

Figure 2: Diffractive DIS in the proton rest frame (left) and the Breit frame (right); asymmetric quark fluctuations correspond to diffractive quark scattering, asymmetric gluon fluctuations to diffractive boson-gluon fusion.

where

$$t_{ij}(y_\perp) = \delta_{ij} - 2\frac{y_i y_j}{y^2} \; . \tag{17}$$

The physical content of both expressions is rather transparent. The modified Bessel functions contain the kinematic effects due to the propagators of the partons penetrating the colour field and the Wilson loops represent the interaction with the proton. Figure 2 illustrates the correspondence between the semiclassical and parton model view of the leading-order processes testing diffractive quark and gluon distributions.

To illustrate the close similarity of diffractive and inclusive scattering in the semiclassical approach, it is instructive to evaluate the diffractive contribution to the inclusive quark distribution. To achieve this, one sets $x = b\xi$ and integrates over ξ keeping x fixed,

$$q_D(x) = \int_x^1 d\xi \frac{dq(x/\xi,\xi)}{d\xi} \; . \tag{18}$$

After neglecting terms $\mathcal{O}(x)$ and exchanging the integration variable ξ for N^2, the $k'_\perp$ integration can be performed trivially. As a consequence, the integrand is evaluated at $y_\perp = y'_\perp$, giving the simple result

$$xq_D(x) = \frac{2}{(2\pi)^4 N_c} \int N^2 dN^2 \int_{y_\perp} K_1(yN)^2 \int_{x_\perp} \mathrm{tr} W^{\mathcal{F}}_{x_\perp}(y_\perp) \mathrm{tr} W^{\mathcal{F}\dagger}_{x_\perp}(y_\perp) \; . \tag{19}$$

This expression can also be obtained from Eq. (3) by the substitution

$$\mathrm{tr}\left(W^{\mathcal{F}}_{x_\perp}(y_\perp) W^{\mathcal{F}\dagger}_{x_\perp}(y_\perp)\right) \to \frac{1}{N_c} \mathrm{tr} W^{\mathcal{F}}_{x_\perp}(y_\perp) \mathrm{tr} W^{\mathcal{F}\dagger}_{x_\perp}(y_\perp) \, . \tag{20}$$

After this substitution, the N^2 integration in Eq. (3) becomes UV-finite, so that the upper limit μ^2 can be dropped; the $\ln Q^2$ term disappears since $\mathrm{tr}\,\partial_{y_\perp} W^{\mathcal{F}}_{x_\perp}(0) = 0$. The above relation between the inclusive and diffractive quark distribution illustrates most clearly the basic idea of the semiclassical approach: diffractive and non-diffractive events are both induced by the interaction of the soft proton colour field with a partonic fluctuation of the incoming virtual photon. The different final states are realized by projecting the outgoing partonic system onto different colour configurations.

Let us finally note that the semiclassical formulae for diffractive parton distributions [8] used in this paper are sufficiently general to accommodate different models of the hadron colour field. For example, they can serve as an alternative starting point for the derivation of the perturbatively generated distributions of [14], where a heavy quark-antiquark fluctuation of a photon was used as a model for the target. Taking the colour field responsible for $\mathrm{tr}W\mathrm{tr}W^\dagger$ in Eqs. (14) and (16) to be the perturbative field of a small dipole configuration, the results of [14] are exactly reproduced (cf. Appendix B). However, the analysis of the present paper is based on the fundamentally non-perturbative model described in the next section.

4 A Model for the gluon field averaging

The averaging over the gluon field configurations of the target discussed in the two previous sections is a complicated operation depending on the full details of the non-perturbative hadronic state. However, in the special case of a very large target, a quantitative treatment becomes possible under minimal additional assumptions.

McLerran and Venugopalan have observed that the large size of a hadronic target, realized, e.g., in an extremely heavy nucleus, introduces a new hard scale into the process of DIS [11]. From the target rest frame point of view, this means that the typical transverse size of the partonic fluctuations of the virtual photon remains perturbative [12], thus justifying the omission of higher Fock states in the semiclassical calculation. Note that this does not imply a complete reduction to perturbation theory since the long distance which the partonic fluctuation travels in the target compensates for its small transverse size, thus requiring the eikonalization of gluon exchange.

Within this framework, it is natural to introduce the additional assumption that the gluonic fields encountered by the partonic probe in distant regions of the target are not correlated (cf. [16] and the somewhat simplified discussion in [12]). Thus, one arrives at the situation depicted in Fig. 3, where a colour dipole passes a large number of regions, each one of size $\sim 1/\Lambda$, with mutually uncorrelated colour fields $A_1 \ldots A_n$.

Consider the fundamental quantity $W_{x_\perp}(y_\perp)_{ij}[A]\, W^\dagger_{x_\perp}(y'_\perp)_{kl}[A]$ which, after specifying the required representation and appropriately contracting the colour indices $ijkl$, enters the formulae for inclusive and diffractive parton distributions. According to Eq. (2), this quantity is the sum of four terms, the most complicated of which involves four U

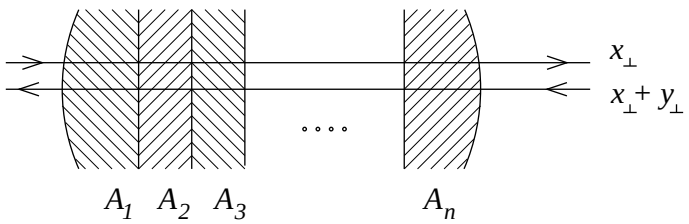

Figure 3: Colour dipole travelling through a large hadronic target.

matrices,

$$\Big\{U_{x_\perp}[A]\,U^\dagger_{x_\perp+y_\perp}[A]\Big\}_{ij}\,\Big\{U_{x_\perp+y'_\perp}[A]\,U^\dagger_{x_\perp}[A]\Big\}_{kl} \tag{21}$$
$$= \Big\{U_{x_\perp}[A_n]\cdots U_{x_\perp}[A_1]\;\; U^\dagger_{x_\perp+y_\perp}[A_1]\cdots U^\dagger_{x_\perp+y_\perp}[A_n]\Big\}_{ij}$$
$$\times\Big\{U_{x_\perp+y'_\perp}[A_n]\cdots U_{x_\perp+y'_\perp}[A_1]\;\; U^\dagger_{x_\perp}[A_1]\cdots U^\dagger_{x_\perp}[A_n]\Big\}_{kl}\,.$$

The crucial assumption that the fields in regions 1 ... n are uncorrelated is implemented by writing the integral over all field configurations as

$$\int_A = \int_{A_1}\cdots\int_{A_n}\,, \tag{22}$$

i.e., as a product of independent integrals. Here the appropriate weighting provided by the target wave functional is implicit in the symbol $\int_A$.

Under the integration specified by Eq. (22), the U matrices on the r.h. side of Eq. (21) can be rearranged to give the result

$$\int_A \Big\{U_{x_\perp}[A]\,U^\dagger_{x_\perp+y_\perp}[A]\Big\}_{ij}\,\Big\{U_{x_\perp+y'_\perp}[A]\,U^\dagger_{x_\perp}[A]\Big\}_{kl} \tag{23}$$
$$= \int_{A_1}\cdots\int_{A_n}\Big\{U_{x_\perp}[A_1]\;U^\dagger_{x_\perp+y_\perp}[A_1]\cdots U_{x_\perp}[A_n]\;U^\dagger_{x_\perp+y_\perp}[A_n]\Big\}_{ij}$$
$$\times\Big\{U_{x_\perp+y'_\perp}[A_n]\;U^\dagger_{x_\perp}[A_n]\cdots U_{x_\perp+y'_\perp}[A_1]\;U^\dagger_{x_\perp}[A_1]\Big\}_{kl}\,.$$

To see this, observe that the A_1 integration acts on the integrand $\{U_{x_\perp}[A_1]\,U^\dagger_{x_\perp+y_\perp}[A_1]\}_{i'j'}$ $\{U_{x_\perp+y'_\perp}[A_1]\,U^\dagger_{x_\perp}[A_1]\}_{k'l'}$ transforming it into an invariant colour tensor with the indices $i'j'k'l'$. The neighbouring matrices $U_{x_\perp}[A_2]$ and $U^\dagger_{x_\perp}[A_2]$ can now be commuted through this tensor structure in such a way that the expression $\{U_{x_\perp}[A_2]\,U^\dagger_{x_\perp+y_\perp}[A_2]\}_{i''j''}$ $\{U_{x_\perp+y'_\perp}[A_2]\,U^\dagger_{x_\perp}[A_2]\}_{k''l''}$ emerges. Subsequently, the A_2 integration transforms this expression into an invariant tensor with indices $i''j''k''l''$. Repeating this argument, one eventually arrives at the structure displayed on the r.h. side of Eq. (23).

To evaluate Eq. (23) further, observe that it represents a contraction of n identical tensors

$$F_{ijkl} = \int_{A_m}\{U_{x_\perp}[A_m]\,U^\dagger_{x_\perp+y_\perp}[A_m]\}_{ij}\,\{U_{x_\perp+y'_\perp}[A_m]\,U^\dagger_{x_\perp}[A_m]\}_{kl}\,, \tag{24}$$

where the index m refers to any one of the regions 1 ... n into which the target is subdivided. At this point, we make use of the fact that for a sufficiently large target the

transverse separations $y_\perp$ and $y'_\perp$ are always small [12]. In fact, for a target of geometrical size $\sim n/\Lambda$ (where $n \gg 1$), the relevant transverse distances are bounded by $y^2 \sim y'^2 \sim 1/n\Lambda^2$.

Assuming that size and $x_\perp$ dependence of typical field configurations A_m are characterized by the scale Λ, it follows that the products $U_{x_\perp} U^\dagger_{x_\perp+y_\perp}$ and $U_{x_\perp+y'_\perp} U^\dagger_{x_\perp}$ are close to unit matrices for all relevant $y_\perp$ and $y'_\perp$. Therefore, it is justified to write

$$U_{x_\perp}[A_m]\, U^\dagger_{x_\perp+y_\perp}[A_m] = \exp\left\{iT^a f^a(x_\perp, y_\perp)[A_m]\right\}, \tag{25}$$

where T^a are the conventional group generators and f^a are functions of $x_\perp$ and $y_\perp$ and functionals of A_m. Equation (25) and its $y'_\perp$ analogue are expanded around $y_\perp = y'_\perp = 0$ (which corresponds to $f^a(x_\perp, 0) = 0$) and inserted into Eq. (24). At leading non-trivial order, the result reads

$$F_{ijkl} = \delta_{ij}\delta_{kl}\left(1 - \frac{1}{2}\gamma C_R(y^2 + y'^2)\right) + \gamma(y_\perp y'_\perp) T^a_{ij} T^a_{kl}\,, \tag{26}$$

where C_R is the Casimir number of the relevant representation ($C_R = C_{F,A}$) and γ is defined by

$$\int_A f^a(x_\perp, y_\perp) f^b(x_\perp, y'_\perp) = \gamma\delta^{ab}(y_\perp y'_\perp) + \mathcal{O}(y^2 y'^2)\,. \tag{27}$$

Note that the absence of terms linear in f^a and the simple structure on the r.h. side of Eq. (27) are enforced by colour covariance and transverse space covariance. The absence of an explicit $x_\perp$ dependence is a consequence of the homogeneity that we assume to hold over the large transverse size of the target. Neglecting boundary effects, we can account for the $x_\perp$ integration by multiplying the final result with a parameter $\Omega \sim n^2/\Lambda^2$ that characterizes the geometrical cross section of the target.

Substituting the n tensors F_{ijkl} on the r.h. side of Eq. (23) by the expression given in Eq. (26) and contracting the colour indices as appropriate for the inclusive and diffractive case respectively, one obtains, in the large-N_c limit,

$$\int_A \left\{U_{x_\perp} U^\dagger_{x_\perp+y_\perp}\right\}_{ij} \left\{U_{x_\perp+y'_\perp} U^\dagger_{x_\perp}\right\}_{ji} = d_R\left[1 - \frac{1}{2}\gamma C_R(y_\perp - y'_\perp)^2\right]^n, \tag{28}$$

$$\int_A \left\{U_{x_\perp} U^\dagger_{x_\perp+y_\perp}\right\}_{ii} \left\{U_{x_\perp+y'_\perp} U^\dagger_{x_\perp}\right\}_{jj} = d_R^2\left[1 - \frac{1}{2}\gamma C_R(y_\perp^2 + y_\perp'^2)\right]^n, \tag{29}$$

where d_R is the dimension of the representation.

Since n is assumed to be large and the typical values of y^2 and y'^2 do not exceed $1/n\Lambda^2$, the formula $(1 - x/n)^n \simeq \exp[-x]$ can be applied to the r.h. sides of Eqs. (28) and (29). Furthermore, contributions proportional to $\{U_{x_\perp} U^\dagger_{x_\perp+y_\perp}\}_{ij}\delta_{kl}\,, \quad \delta_{ij}\{U_{x_\perp+y'_\perp} U^\dagger_{x_\perp}\}_{kl}$ and $\delta_{ij}\delta_{kl}$ have to be added to obtain the complete expression for $W_{x_\perp}(y_\perp)_{ij}\, W^\dagger_{x_\perp}(y'_\perp)_{kl}$. The corresponding calculations are straightforward and the result reads

$$\int_{x_\perp}\int_A \mathrm{tr}\left(W_{x_\perp}(y_\perp) W^\dagger_{x_\perp}(y'_\perp)\right) = \Omega d_R\left[1 - e^{-a_R y^2} - e^{-a_R y'^2} + e^{-a_R(y_\perp - y'_\perp)^2}\right], \tag{30}$$

$$\int_{x_\perp}\int_A \mathrm{tr} W_{x_\perp}(y_\perp)\mathrm{tr} W^\dagger_{x_\perp}(y'_\perp) = \Omega d_R^2\left[1 - e^{-a_R y^2}\right]\left[1 - e^{-a_R y'^2}\right], \tag{31}$$

where $a_R = n\gamma C_R/2$ plays the role of a saturation scale.

The above calculation, performed at large N_c and for the case of a large target subdivided into many uncorrelated regions, has no immediate application to realistic experiments. However, it provides us with a set of non-perturbative inclusive and diffractive parton distributions which are highly constrained with respect to each other. Assuming that some of the essential features of diffractive and inclusive DIS are common to both the above model and the realistic proton case, we use the basic formulae Eq. (30) and (31) for a phenomenological analysis. For this purpose, Ω and $a \equiv n\gamma N_c/4$ are considered as new fundamental parameters, giving rise to the following formulae for the basic hadronic quantities required in Sections 2 and 3,

$$\int_{x_\perp}\int_A \mathrm{tr}\left(W^{\mathcal{F}}_{x_\perp}(y_\perp)W^{\mathcal{F}\dagger}_{x_\perp}(y'_\perp)\right) = \Omega N_c\left[1-e^{-ay^2}-e^{-ay'^2}+e^{-a(y_\perp-y'_\perp)^2}\right], \quad (32)$$

$$\frac{1}{N_c}\int_{x_\perp}\int_A \mathrm{tr}W^{\mathcal{F}}_{x_\perp}(y_\perp)\mathrm{tr}W^{\mathcal{F}\dagger}_{x_\perp}(y'_\perp) = \Omega N_c\left[1-e^{-ay^2}\right]\left[1-e^{-ay'^2}\right], \quad (33)$$

$$\frac{1}{N_c^2}\int_{x_\perp}\int_A \mathrm{tr}W^{\mathcal{A}}_{x_\perp}(y_\perp)\mathrm{tr}W^{\mathcal{A}\dagger}_{x_\perp}(y'_\perp) = \Omega N_c^2\left[1-e^{-2ay^2}\right]\left[1-e^{-2ay'^2}\right]. \quad (34)$$

A similar, Glauber type y^2 dependence has been recently used in the DIS analysis of [17]. Note that according to Eqs. (32)–(34) the diffractive structure function is not suppressed by a colour factor relative to the inclusive structure function, as originally suggested in [18].

5 Numerical analysis

The model of the previous section provides an example for the relation between diffractive and inclusive parton distributions in the semiclassical approach. Although the derivation was based on a large hadronic target (with radius much greater than $1/\Lambda$), we expect some qualitative features of the resulting distributions to apply to the proton as well. The above model distributions are used as non-perturbative input at some small scale Q_0^2 and are evolved to higher Q^2 using the leading-order DGLAP equations [10]. The non-perturbative parameters of the model, as well as the scale Q_0^2, are then determined from a combined analysis of experimental data on inclusive and diffractive structure functions.

At first sight, the semiclassical description of parton distribution functions always predicts an energy dependence corresponding to a classical bremsstrahlung spectrum: $q(x), g(x) \sim 1/x$. However, this naïve prediction assumes the averaging over the soft field configurations inside the proton to be independent of the energy of the quark pair used to probe these configurations. As already outlined in Sect. 2, one expects that, in a more complete treatment, a non-trivial energy dependence is induced since the averaging procedure encompasses more and more modes of the proton field with increasing energy of the probe. We are, however, unable to calculate this non-perturbative energy dependence from first principles. Instead, we choose to parametrize it in the form of a soft, logarithmic growth of the normalization of diffractive and inclusive parton distributions with the

collision energy $\sim 1/x$, consistent with the unitarity bound. This introduces one further parameter, L, into the model:

$$\Omega \to \Omega \, (L - \ln x)^2 \, . \tag{35}$$

Including this energy dependence, our model yields the following compact expressions for the semiclassical inclusive parton distributions Eqs. (3),(4) at a low scale Q_0^2:

$$xq(x,Q_0^2) \;=\; \frac{a\Omega N_c \, (L-\ln x)^2}{3\pi^3} \left(\ln \frac{Q_0^2}{a} - 0.6424 \right) \, , \tag{36}$$

$$xg(x,Q_0^2) \;=\; \frac{2a\Omega N_c \, (L-\ln x)^2}{\pi^2 \alpha_s(Q_0^2)} \, . \tag{37}$$

Being derived in the semiclassical approach, these expressions are only valid in the small-x region, which we define by $x \leq 0.01$. In our numerical analysis, we shall multiply the above expressions with $(1-x)$ to ensure vanishing of the distributions in the limit $x \to 1$, which is required for the numerical stability of the DGLAP evolution.

The corresponding expressions for the diffractive distributions Eqs. (14),(16) can be derived in a similar manner. The integrations over the momentum variables are outlined in Appendix A. One is then left with the expressions

$$\frac{dq \, (\beta,\xi,Q_0^2)}{d\xi} \;=\; \frac{a\Omega N_c (1-\beta) \, (L-\ln \xi)^2}{2\pi^3 \xi^2} f_q(\beta) \, , \tag{38}$$

$$\frac{dg \, (\beta,\xi,Q_0^2)}{d\xi} \;=\; \frac{a\Omega N_c^2 (1-\beta)^2 \, (L-\ln \xi)^2}{2\pi^3 \beta \xi^2} f_g(\beta) \, , \tag{39}$$

with the functions $f_{q,g}(\beta)$ being defined in Appendix A. The β spectrum of the diffractive parton distributions at Q_0^2 is independent of the unknown non-perturbative parameters. Note that our model does not specify whether, in the diffractive case, the energy-dependent logarithm should be a function of x or of ξ. However, both prescriptions differ only by terms proportional to $\ln \beta$, which can be disregarded in comparison with $\ln x$ or $\ln \xi$ in the small-x region. Like their inclusive counterparts, these distributions are only valid in the region $\xi \leq 0.01$, where we believe the semiclassical approach to apply.

The above equations summarize our input distributions, depending on a, Ω, L, and on the scale Q_0^2, at which these distributions will be used as boundary condition for the leading-order DGLAP evolution. At this order, the measured structure function F_2 coincides with the transverse structure function discussed in Sects. 2 and 3. In defining structure functions and parton distributions, we assume all three light quark flavours to yield the same contribution, such that the singlet quark distribution is simply six times the quark distribution defined above, both in the inclusive and in the diffractive case:

$$\Sigma(x,Q^2) = 6 \, q(x,Q^2) \, , \qquad \frac{d\,\Sigma(\xi,\beta,Q^2)}{d\xi} = 6 \, \frac{dq(\xi,\beta,Q^2)}{d\xi} \, . \tag{40}$$

Valence quark contributions are absent in the semiclassical approach, which does not account for the exchange of flavour quantum numbers between the proton and the fast moving virtual photon state.

Charm quarks are treated entirely as massive quarks in the fixed flavour number scheme [19], which is appropriate since, in the Q^2 range under consideration, charm threshold effects are far more important than the resummation of $\ln Q^2/m_c^2$ terms. We thus fix $n_f = 3$ in the DGLAP splitting functions and evolve only gluon and singlet quark distribution. The structure functions F_2 and $F_2^{D(3)}$ are then given by the singlet quark distribution and a massive charm quark contribution due to boson-gluon fusion. Explicit formulae can, for example, be found in [5]. For our numerical studies we use $\Lambda_{\mathrm{LO},n_f=3} = 144$ MeV ($\alpha_s(M_Z) = 0.118$), $m_c = 1.5$ GeV, $m_b = 4.5$ GeV, and we evaluate the massive charm quark contribution for a renormalization and factorization scale $\mu_c = 2m_c$.

The resulting structure functions can be compared with HERA data on the inclusive structure function $F_2(x, Q^2)$ [1] and on the diffractive structure function $F_2^{D(3)}(\xi, \beta, Q^2)$ [2]. These data sets from the H1 and ZEUS experiments are used to determine the unknown parameters of our model. We apply the following selection criteria to the data: $x \leq 0.01$ and $\xi \leq 0.01$ are needed to justify the semiclassical description of the proton colour field; with Q_0^2 being a fit parameter, we demand a sufficiently large minimum $Q^2 = 2$ GeV^2 to avoid that the data selection is influenced by the current value of Q_0^2; finally we require $M^2 > 4$ GeV^2 in the diffractive case to justify the leading-twist analysis.

We determine the optimum set of model parameters from a minimization of the total χ^2 (based on statistical errors only) of the selected data, using the MINUIT package [20]. The resulting set of parameters is

$$\begin{aligned} Q_0^2 &= 1.23 \text{ GeV}^2 , \\ L &= 8.16 , \\ \Omega &= (712 \text{ MeV})^{-2} , \\ a &= (74.5 \text{ MeV})^2 . \end{aligned} \tag{41}$$

The distributions obtained with these fitted parameters yield a good qualitative description of all data on inclusive and diffractive DIS at small x, as illustrated in Figs. 4, 5 and 6. All parameters are given with a precision which allows to reproduce the plots, but which is inappropriate with respect to the crudeness of the model. The starting scale Q_0^2 is in the region where one would expect the transition between perturbative and non-perturbative dynamics to take place; the two other dimensionful parameters ΩL^2 and a are both of the order of typical hadronic scales.

Our approach fails to reproduce the data on $F_2^{D(3)}$ for low M^2 (open dots in Figs. 5 and 6). This might indicate the importance of higher twist contributions in this region, as suggested in [6]. It is interesting to note that a breakdown of the leading twist description is also observed for inclusive structure functions [21], where it occurs for similar invariant hadronic masses, namely $W^2 \lesssim 4$ GeV^2.

The perturbative evolution of inclusive and diffractive structure functions is driven by the gluon distribution, which is considerably larger than the singlet quark distribution in both cases. The ratio of the inclusive singlet quark and gluon distributions can be read off from Eqs. (36) and (37). With the fit parameters obtained above, it turns out that the

inclusive gluon distribution is about twice as large as the singlet quark distribution. In contrast, the relative magnitude and the β dependence of the diffractive distributions are completely independent of the model parameters. Moreover, their absolute normalization is, up to the slowly varying factor $1/\alpha_s(Q_0^2)$, closely tied to the normalization of the inclusive gluon distribution.

Figure 7 displays the diffractive distributions (multiplied by β and thus reflecting the distribution of momentum carried by the partons) for fixed $\xi = 0.003$ and different values of Q^2. The β dependences of the quark and the gluon distribution at Q_0^2 are substantially different: the quark distribution $\beta d\Sigma/d\xi$ is peaked around $\beta \approx 0.65$, thus being harder than the distribution $\beta(1-\beta)$ suggested in [22]. It vanishes like β for $\beta \to 0$ and like $(1-\beta)$ at large β; the gluon distribution $\beta dg/d\xi$, on the other hand, approaches a constant for $\beta \to 0$ and falls off like $(1-\beta)^2$ at large β. This asymptotic behaviour in the small- and large-β region is in agreement with the results obtained in the perturbative approach of [14]. In spite of the $(1-\beta)^2$ behaviour, gluons remain important even at large β, simply due to the large total normalization of this distribution (the β integral over $\beta dg/d\xi$ at Q_0^2 is approximately three times the β integral over $\beta d\Sigma/d\xi$). As a result, the quark distribution does not change with increasing Q^2 for $\beta \approx 0.5$ and is only slowly decreasing for larger values of β.

The dependence of the diffractive structure function on β and Q^2 is illustrated in Fig. 8, where we compare our predictions with data from the H1 and ZEUS experiments [2] at fixed $\xi = 0.003$ (H1) and $\xi = 0.0042$ (ZEUS). It must be pointed out that these data points are based on a combination of data taken at various values of ξ (including $\xi > 0.01$), which have been extrapolated to fixed ξ. The energy dependence of the diffractive structure function used for this extrapolation is different from the energy dependence employed in our model, so that a detailed comparison of the data with our results should only be made with some caution. Disregarding the large-β region, our model gives a good description of the β dependence of the diffractive structure function for all values of Q^2.

The validity of our approach can be tested by studying DIS observables other than the diffractive structure function $F_2^{D(3)}$ used to fit our model parameters. In particular, it would be of interest to study quantities which are directly proportional to the diffractive gluon distribution, such as the charm content of $F_2^{D(3)}$. The dashed lines in Fig. 8 show our prediction for the diffractive charm structure function due to photon-gluon fusion. Moreover, this structure function is predicted to have the same, non-perturbative ξ dependence as $F_2^{D(3)}(\xi, \beta, Q^2)$. The charm contribution is sizeable in the small-β region. Since the full diffractive cross section at fixed x is obtained after integration with the measure $d\beta/\beta$, this region yields a substantial diffractive charm cross section.

The β dependence of diffractive parton distributions used in the present numerical analysis is a direct result of our specific model for the colour field averaging. It would therefore be very interesting to repeat the analysis with more sophisticated models, such as the stochastic vacuum model that was utilized for diffractive meson production in [23].

6 Conclusions

In the target rest frame, DIS at small x can be viewed as the interaction of a partonic fluctuation of the virtual photon with the proton colour field. The semiclassical approach assumes this proton field to be dominated by soft modes, which have the sole effect of introducing a non-Abelian phase factor for each parton. In this approach, a very similar description of inclusive and diffractive events emerges, the latter being realized if the partonic fluctuation leaves the proton in a colour singlet state. Inclusive and diffractive structure functions are therefore calculated by evaluating different colour contractions of the same soft scattering amplitudes.

Matching the semiclassical and partonic description of structure functions at some low scale Q_0^2, where logarithmic corrections are still small, a set of semiclassical parton distribution functions for inclusive and diffractive processes is defined. The evolution to higher scales is then determined by the conventional leading-order DGLAP equations. Initial quark and gluon distributions are expressed in terms of averages over the proton colour field.

In the semiclassical framework, a very special role is played by the inclusive gluon distribution. In contrast to both the inclusive quark distribution and the diffractive quark and gluon distributions, it is only sensitive to the short distance structure of the proton field, and it is enhanced by an explicit factor $1/\alpha_s$. As a result, the observed dominance of the inclusive over the diffractive DIS cross section emerges.

To study the semiclassical distributions in more detail, we introduce a non-perturbative model for the proton colour field. This model is derived for a very large hadronic target, which can be subdivided into different zones of uncorrelated colour field strengths. A non-trivial example of a non-perturbative set of semiclassical distributions results. In spite of its lacking theoretical justification in the case of a proton target, this set of distributions can serve as a basis of a phenomenological analysis. Our model depends on two free parameters which are related to the average field strength in a zone and to the total geometrical size of the target. A further parameter has to be introduced to account for the unknown energy dependence induced by the averaging over the field configurations. Thus, our model describes all semiclassical parton distributions by three unknown non-perturbative parameters and the matching scale Q_0^2.

These three model parameters and Q_0^2 are determined from a combined fit to measurements of inclusive [1] and diffractive [2] structure functions at small x. The resulting distributions yield a satisfactory description of the structure functions $F_2(x, Q^2)$ and $F_2^{D(3)}(\xi, \beta, Q^2)$. It turns out that the Q^2 evolution of both structure functions is mainly driven by large gluon distributions.

The good agreement of our model with the experimental data allows us to conclude that both inclusive and diffractive DIS at small x can be described in a unified picture in the semiclassical approach. A simple model for the colour field averaging, adopted from a large target, is used to compute the semiclassical parton distributions at some initial scale Q_0^2. The behaviour above Q_0^2 is then determined by perturbative evolution at leading order in α_s and leading twist.

The rise of $F_2(x,Q^2)$ and of $F_2^{D(3)}(\xi,\beta,Q^2)$ at small x have the same, *non-perturbative* origin in the energy dependence of the average over soft field configurations in the proton. With increasing Q^2, this rise is enhanced by perturbative evolution in the case of the inclusive structure function, while it remains unchanged in the diffractive structure function.

The obtained parton distributions can be used to predict a broad spectrum of observables in diffractive and inclusive processes using standard methods of perturbative QCD. The qualitative relation between diffractive and inclusive DIS and the universal ξ dependence of large-mass diffraction are genuine predictions of the semiclassical approach. By contrast, the β dependence of the diffractive distributions is a result of our specific model for the colour field averaging. Crucial tests of this model can be performed in future measurements of diffractive final states. At the same time, other models for the averaging procedure can be tested in the present framework.

We would like to thank M.F. McDermott, B.R. Webber and H. Weigert for valuable discussions and comments.

Appendix A: Diffractive parton distributions

In the following, we collect several formulae which are useful in connection with the semiclassical expressions for the diffractive parton distributions (Sect. 3) and with their explicit evaluation within our model of the proton colour field (Sect. 4).

In Ref. [8], the diffractive quark distribution was given in the form

$$\frac{dq(b,\xi)}{d\xi} = \frac{2}{\xi^2(1-b)^2}\int\frac{d^2k'_\perp\,k'^2}{(2\pi)^8 N_c}\int_{x_\perp}\left|\int\frac{d^2k_\perp\,k_\perp}{uk'^2+k^2}\int_{y_\perp}e^{i(k'_\perp-k_\perp)y_\perp}\mathrm{tr}W^{\mathcal{F}}_{x_\perp}(y_\perp)\right|^2 , \qquad (42)$$

where $u = b/(1-b)$. Starting from this result, Eq. (14) of Sect. 3 can be derived using the identity

$$\int\frac{d^2k_\perp}{(2\pi)^2}\frac{k_i e^{ik_\perp y_\perp}}{N^2+k_\perp^2} = \frac{i}{2\pi}\frac{y_i}{y}NK_1(yN) . \qquad (43)$$

For the phenomenological analysis, we use the specific model of Sect. 4. Inserting for $\mathrm{tr}W^{\mathcal{F}}_{x_\perp}(y_\perp)\mathrm{tr}W^{\mathcal{F}\dagger}_{x_\perp}(y'_\perp)$ in Eq. (42) the expression from Eq. (33), the $y_\perp$ integration and some of the momentum integrations can be carried out. The result reads

$$\frac{dq(b,\xi)}{d\xi} = \frac{a\Omega N_c(1-b)}{2\pi^3\xi^2}f_q(b) , \qquad (44)$$

where $f_q(b)$ is an integral over two Feynman-type parameters,

$$f_q(b) = 4\int_0^\infty dxdx'\frac{\left(\frac{\sqrt{b}+x}{(1-b+(\sqrt{b}+x)^2)^2}\right)\left(\frac{\sqrt{b}+x'}{(1-b+(\sqrt{b}+x')^2)^2}\right)}{(x+x')\sqrt{b}+(1-b)\left(\frac{x}{\sqrt{b}+x}+\frac{x'}{\sqrt{b}+x'}\right)} . \qquad (45)$$

We were not able to obtain an analytical expression for this integral. It is, however, easily evaluated at $b = 0$ and $b = 1$ yielding $f_q(0) = 1/2$ and $f_q(1) = 3\pi^2/8 - 2$.

Similar formulae hold for the diffractive gluon distribution. The result of [8] reads

$$\frac{dg(b,\xi)}{d\xi} = \frac{b}{\xi^2(1-b)^3} \int \frac{d^2k'_\perp\, k'^4}{(2\pi)^8 N_c^2} \int_{x_\perp} \left| \int \frac{d^2k_\perp\, t_{ij}}{uk'^2 + k^2} \int_{y_\perp} e^{i(k'_\perp - k_\perp)y_\perp} \mathrm{tr} W^{\mathcal{A}}_{x_\perp}(y_\perp) \right|^2 , \qquad (46)$$

where

$$t_{ij} = \delta_{ij} + 2\frac{k_i k_j}{uk'^2} . \qquad (47)$$

Using

$$\int \frac{d^2k_\perp}{(2\pi)^2} \left(\delta_{ij} + 2\frac{k_i k_j}{N^2}\right) \frac{e^{ik_\perp y_\perp}}{N^2 + k_\perp^2} = \frac{1}{2\pi} \left(\delta_{ij} - 2\frac{y_i y_j}{y^2}\right) K_2(yN) , \qquad (48)$$

one obtains Eq. (16) in Sect. 3. Inserting for $\mathrm{tr} W^{\mathcal{A}}_{x_\perp}(y_\perp) \mathrm{tr} W^{\mathcal{A}\dagger}_{x_\perp}(y'_\perp)$ the expression in Eq. (34) of Sect. 4, the $y_\perp$ integration and some of the momentum integrations can be carried out. The result has the same structure as the diffractive quark distribution,

$$\frac{dg(b,\xi)}{d\xi} = \frac{a\Omega N_c^2 (1-b)^2}{2\pi^3 \xi^2 b} f_g(b) , \qquad (49)$$

where $f_g(b)$ is given by the two-dimensional integral

$$f_g(b) = 2\int_0^\infty dx dx' \frac{\left(\frac{1-b+3(1+x)^2 b}{(1+x)^2(1-b+(1+x)^2 b)^2}\right)\left(\frac{1-b+3(1+x')^2 b}{(1+x')^2(1-b+(1+x')^2 b)^2}\right)}{(x+x')b + (1-b)\left(\frac{x}{1+x} + \frac{x'}{1+x'}\right)} . \qquad (50)$$

This integral is easily evaluated for $b = 0$ and $b = 1$ yielding $f_g(0) = 4\ln 2$ and $f_g(1) = 45\pi^2/32 - 17/2$. For general b, we have evaluated $f_q(b)$ and $f_g(b)$ only numerically, the results can be inferred from the solid curves in Fig. 7.

Appendix B: Comparison with a perturbative model

It is the purpose of this appendix to outline how the perturbative results of [14] can be derived on the basis of the semiclassical formulae for diffractive parton distributions of [8] (cf. Eqs. (42) and (46) of this paper).

The authors of [14] study diffraction as quasi-elastic scattering off a special target photon that couples to only one flavour of very massive ($M \gg \Lambda$) quarks. The large quark mass justifies a completely perturbative treatment of the target and the diffractive system. In this situation, the required t channel colour singlet exchange is realized by two gluons coupling to the massive quark loop of the target. In the semiclassical approach, these two gluons are understood to be radiated by the massive quark loop and are treated as the colour field generating $\mathrm{tr} W \mathrm{tr} W^\dagger$. The semiclassical calculation proceeds as follows.

Equations (42) and (46) have the structure

$$\frac{df_a}{d\xi} = F_a \left[\int_{x_\perp} \mathrm{tr} W_{x_\perp} \, \mathrm{tr} W^\dagger_{x_\perp} \right] , \tag{51}$$

where F_a (with $a = q, g$) is a linear functional depending on $\int \mathrm{tr} W_{x_\perp}(y_\perp) \, \mathrm{tr} W^\dagger_{x_\perp}(y'_\perp)$, interpreted as a function of $y_\perp$ and $y'_\perp$. To be differential in t, one simply writes

$$\frac{df_a}{d\xi \, dt} = \frac{1}{4\pi} F_a \left[\int_{x_\perp} \int_{x'_\perp} \mathrm{tr} W_{x_\perp} \, \mathrm{tr} W^\dagger_{x'_\perp} e^{iq_\perp (x'_\perp - x_\perp)} \right] , \tag{52}$$

with $q_\perp^2 = -t$.

The field responsible for $\mathrm{tr}W$ is created by a small colour dipole which, in turn, is created by the special photon that models the target. At leading order in perturbation theory, the colour field of a static quark is analogous to its electrostatic Coulomb field. The field of a quark travelling on the light cone in x_- direction ($x_\pm = x_0 \pm x_3$) at transverse position $0_\perp$ has therefore the following line integral along the x_+ direction,

$$-\frac{ig}{2} \int A_- \, dx_+ \; = \; -ig^2 \int \frac{d^2 k_\perp}{(2\pi)^2} \cdot \frac{e^{ik_\perp x_\perp}}{k_\perp^2} \; . \tag{53}$$

It is exactly this type of line integral that appears in the exponents of the non-Abelian phase factors U and $U^\dagger$ that form W (cf. Eq. (3) of [8]). A straightforward calculation shows that the function $\mathrm{tr}W$ produced by a dipole consisting of a quark at $\rho_\perp$ and an antiquark at $0_\perp$ reads

$$\begin{aligned} \mathrm{tr} W_{x_\perp}(y_\perp) \; &= \; -\frac{g^4 (N_c^2 - 1) T_R}{2} \left[\int_{k_\perp, k'_\perp} \frac{\left(1 - e^{-ik_\perp \rho_\perp}\right) \left(1 - e^{-ik'_\perp \rho_\perp}\right)}{(2\pi)^4 k_\perp^2 k_\perp'^2} \right] \\ &\quad \times \left(1 - e^{ik_\perp y_\perp}\right) \left(1 - e^{ik'_\perp y_\perp}\right) \, e^{i(k_\perp + k'_\perp) x_\perp} \, , \end{aligned} \tag{54}$$

where $T_F = 1/2$ and $T_A = N_c$ have to be used for the fundamental and adjoint representation respectively.

The final formulae for the diffractive parton distributions of the target are obtained after integrating over the transverse sizes of the colour dipoles with a weight given by the $q\bar{q}$ wave functions of the incoming and outgoing target photon. They read

$$\begin{aligned} \frac{df_a}{d\xi \, dt} \; &= \; \int dz \, d^2 \rho_\perp \int dz' \, d^2 \rho'_\perp \, \frac{1}{4\pi} F_a \left[\int_{x_\perp} \int_{x'_\perp} \mathrm{tr} W_{x_\perp} \, \mathrm{tr} W^\dagger_{x'_\perp} e^{iq_\perp (x'_\perp - x_\perp)} \right] \\ &\quad \times \frac{1}{2} \sum_{\epsilon, \epsilon'} \left[\psi^*_\gamma(z, \rho_\perp, p'_\perp, \epsilon'_\perp) \, \psi_\gamma(z, \rho_\perp, 0_\perp, \epsilon_\perp) \right] \left[\psi^*_\gamma(z,' \rho'_\perp, p'_\perp, \epsilon'_\perp) \, \psi_\gamma(z', \rho'_\perp, 0_\perp, \epsilon_\perp) \right] , \end{aligned} \tag{55}$$

where $\mathrm{tr}W_{x_\perp}(y_\perp)$ is produced by the field of a quark at $\rho_\perp$ and an antiquark at $0_\perp$, and $\mathrm{tr}W_{x'_\perp}(y'_\perp)$ is produced by the field of a quark at $\rho'_\perp$ and an antiquark at $0_\perp$, as detailed in Eq. (54).

The wave function $\psi_\gamma(z,\rho_\perp,0_\perp,\epsilon_\perp)$ characterizes the amplitude for the fluctuation of the incoming target photon with polarization ϵ and transverse momentum $0_\perp$ into a $q\bar{q}$ pair with momentum fractions z and $1-z$ and transverse separation $\rho_\perp$. Similarly, the wave function $\psi^*_\gamma(z,\rho_\perp,p'_\perp,\epsilon'_\perp)$ characterizes the amplitude for the recombination of this $q\bar{q}$ pair into a photon with polarization ϵ' and transverse momentum $p'_\perp=-q_\perp$. The summation over the helicities of the intermediate quark states, which are conserved by the high-energy gluonic interaction, is implicit.

The required product of photon wave functions can be calculated following the lines of [7,24]. It reads explicitly

$$\psi^*_\gamma(z,\rho_\perp,p'_\perp,\epsilon'_\perp)\,\psi_\gamma(z,\rho_\perp,0_\perp,\epsilon_\perp) \tag{56}$$
$$= \frac{N_c e^2 e_q^2}{2(2\pi)^5}\int_{k_\perp,k'_\perp} \mathrm{tr}\Phi^\dagger(z,k'_\perp,M,\epsilon'_\perp)\Phi(z,k_\perp,M,\epsilon_\perp)e^{i\rho_\perp(k'_\perp-k_\perp+zp'_\perp)}\,,$$

where we have used the notation of [14],

$$\Phi(z,k_\perp,M,\epsilon_\perp)=\frac{1}{(k_\perp^2+M^2)}\left[(1-z)\,\epsilon_\perp\cdot\sigma\,k_\perp\cdot\sigma - z\,k_\perp\cdot\sigma\,\epsilon_\perp\cdot\sigma + iM\,\epsilon_\perp\cdot\sigma\right], \tag{57}$$

M is the quark mass and $\sigma_{1,2}$ are the first two Pauli matrices. Note that for $p'_\perp=0$, the average of the diagonal elements ($\epsilon_\perp=\epsilon'_\perp$) in Eq. (56) reproduces the well known formula for the square of the photon wave function [3].

Inserting Eq. (56) into Eq. (55) and introducing explicitly the required functionals F_a specified by Eqs. (42) and (46), the formulae of [14] for diffractive quark and gluon distribution are exactly reproduced.

References

[1] H1 Collab., S. Aid et al., Nucl. Phys. B470 (1996) 3;
ZEUS Collab., M. Derrick et al., Z. Phys. C72 (1996) 399

[2] H1 Collab., C. Adloff et al., Z. Phys. C76 (1997) 613;
ZEUS Collab., J. Breitweg et al., preprint DESY-98-084 (hep-ex/9807010)

[3] N.N. Nikolaev and B.G. Zakharov, Z. Phys. C49 (1991) 607

[4] K. Golec-Biernat and J. Kwieciński, Phys. Lett. B353 (1995) 329;
A. Edin, G. Ingelman and J. Rathsman, Z. Phys. C75 (1997) 57;
E. Gotsman, E. Levin and U. Maor, Nucl. Phys. B493 (1997) 354;
A. Bialas, R. Peschanski and C. Royon, Phys. Rev. D57 (1998) 6899

[5] T. Gehrmann and W.J. Stirling, Z. Phys. C70 (1996) 89

[6] J. Bartels, J. Ellis, H. Kowalski and M. Wüsthoff, preprint CERN-TH-98-67, DESY 98-034 and DTP-98-02 (hep-ph/9803497)

[7] W. Buchmüller, M.F. McDermott and A. Hebecker, Nucl. Phys. B487 (1997) 283; *ibid.* B500 (1997) 621 (E)

[8] A. Hebecker, Nucl. Phys. B505 (1997) 349

[9] G. Ingelman and P.E. Schlein, Phys. Lett. B152 (1985) 256;
L. Trentadue and G. Veneziano, Phys. Lett. B323 (1994) 201;
A. Berera and D.E. Soper, Phys. Rev D50 (1994) 4328

[10] V.N. Gribov and L.N. Lipatov, Sov. J. Nucl. Phys. 15 (1972) 438, 675;
G. Altarelli and G. Parisi, Nucl. Phys. B126 (1977) 298;
Yu.L. Dokshitzer, Sov. Phys. JETP 46 (1977) 641

[11] L. McLerran and R. Venugopalan, Phys. Rev. D49 (1994) 2233

[12] A. Hebecker and H. Weigert, Phys. Lett. B432 (1998) 215

[13] W. Buchmüller, Phys. Lett. B353 (1995) 335;
W. Buchmüller and A. Hebecker, Nucl. Phys. B476 (1996) 203

[14] F. Hautmann, Z. Kunszt and D.E. Soper, preprint CERN-TH-98-168, ETH-TH/98-14 and OITS 648 (hep-ph/9806298)

[15] J.C. Collins, Phys. Rev. D57 (1998) 3051

[16] J. Jalilian-Marian, A. Kovner, L. McLerran and H. Weigert, Phys. Rev. D55 (1997) 5414

[17] K. Golec-Biernat and M. Wüsthoff, preprint DTP/98/50 (hep-ph/9807513)

[18] W. Buchmüller and A. Hebecker, Phys. Lett. B355 (1995) 573

[19] M. Glück, E. Reya and M. Stratmann, Nucl. Phys. B422 (1994) 37

[20] F. James, MINUIT, CERN Program Library Long Writeup D506 (1994)

[21] A. Milsztajn and M. Virchaux, Phys. Lett. B274 (1992) 221;
A.D. Martin, R.G. Roberts, W.J. Stirling and R.S. Thorne, preprint DTP-98-52 (hep-ph/9808371)

[22] A. Donnachie and P.V. Landshoff, Phys. Lett. B191 (1987) 309; *ibid.* B198 (1987) 590 (E)

[23] H.G. Dosch, O. Nachtmann and M. Rueter, preprint HD-THEP-98-22 and TAUP-2502-98 (hep-ph/9806342)

[24] M. Wüsthoff, Phys. Rev. D56 (1997) 4311

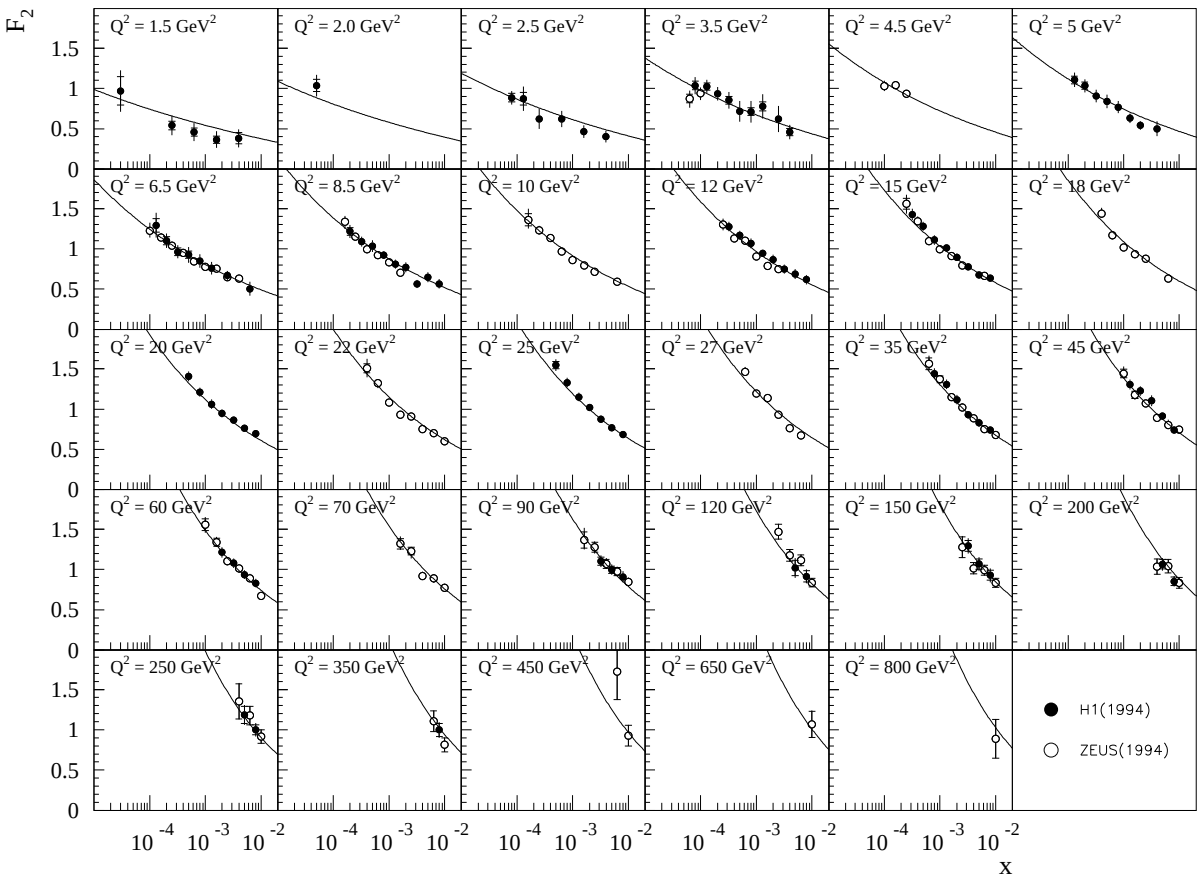

Figure 4: The inclusive structure function $F_2(x, Q^2)$ at small x computed in the semi-classical approach, using the fitted parameters given in the text. Data taken from [1]. The data with $Q^2 = 1.5$ GeV^2 are not included in the fit.

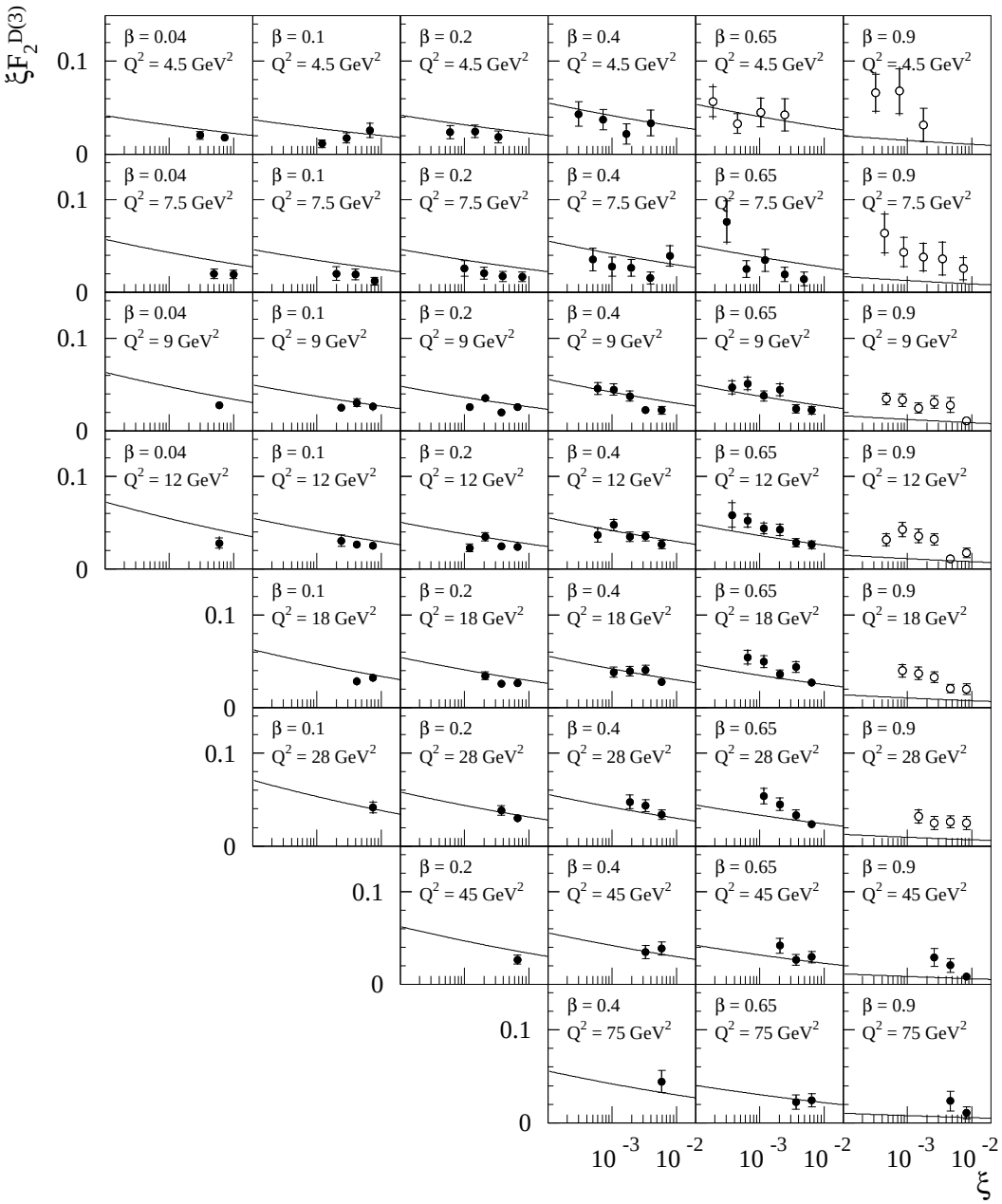

Figure 5: The diffractive structure function $F_2^{D(3)}(\xi, \beta, Q^2)$ at small ξ computed in the semiclassical approach, using the fitted parameters given in the text. H1 data taken from [2]. The open data points correspond to $M^2 \leq 4$ GeV^2 and are not included in the fit.

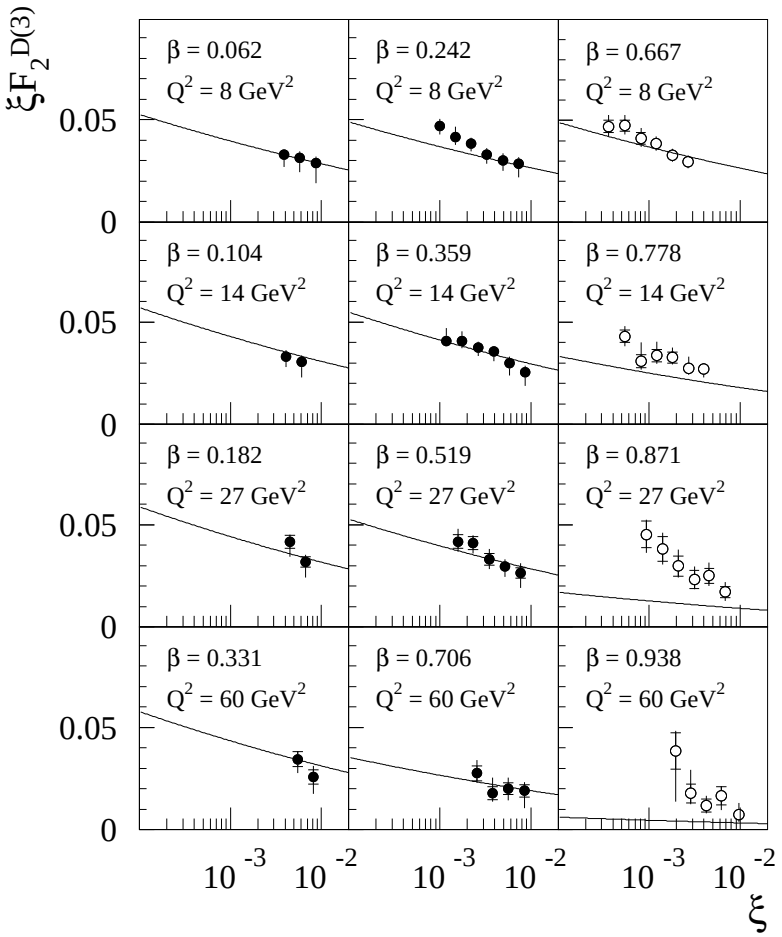

Figure 6: The diffractive structure function $F_2^{D(3)}(\xi, \beta, Q^2)$ at small ξ computed in the semiclassical approach, using the fitted parameters given in the text. ZEUS data taken from [2]. The open data points correspond to $M^2 \leq 4$ GeV^2 and are not included in the fit.

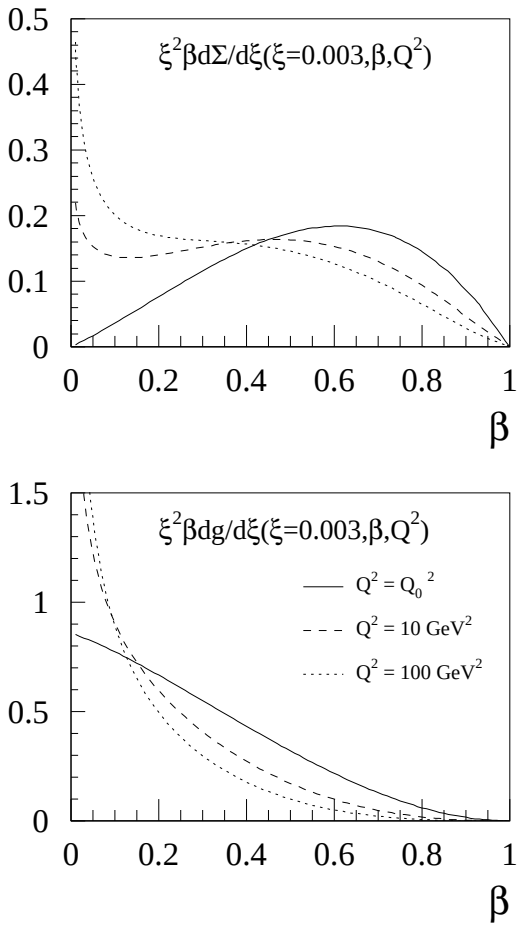

Figure 7: Diffractive quark and gluon distributions at the initial scale Q_0^2 and after Q^2 evolution.

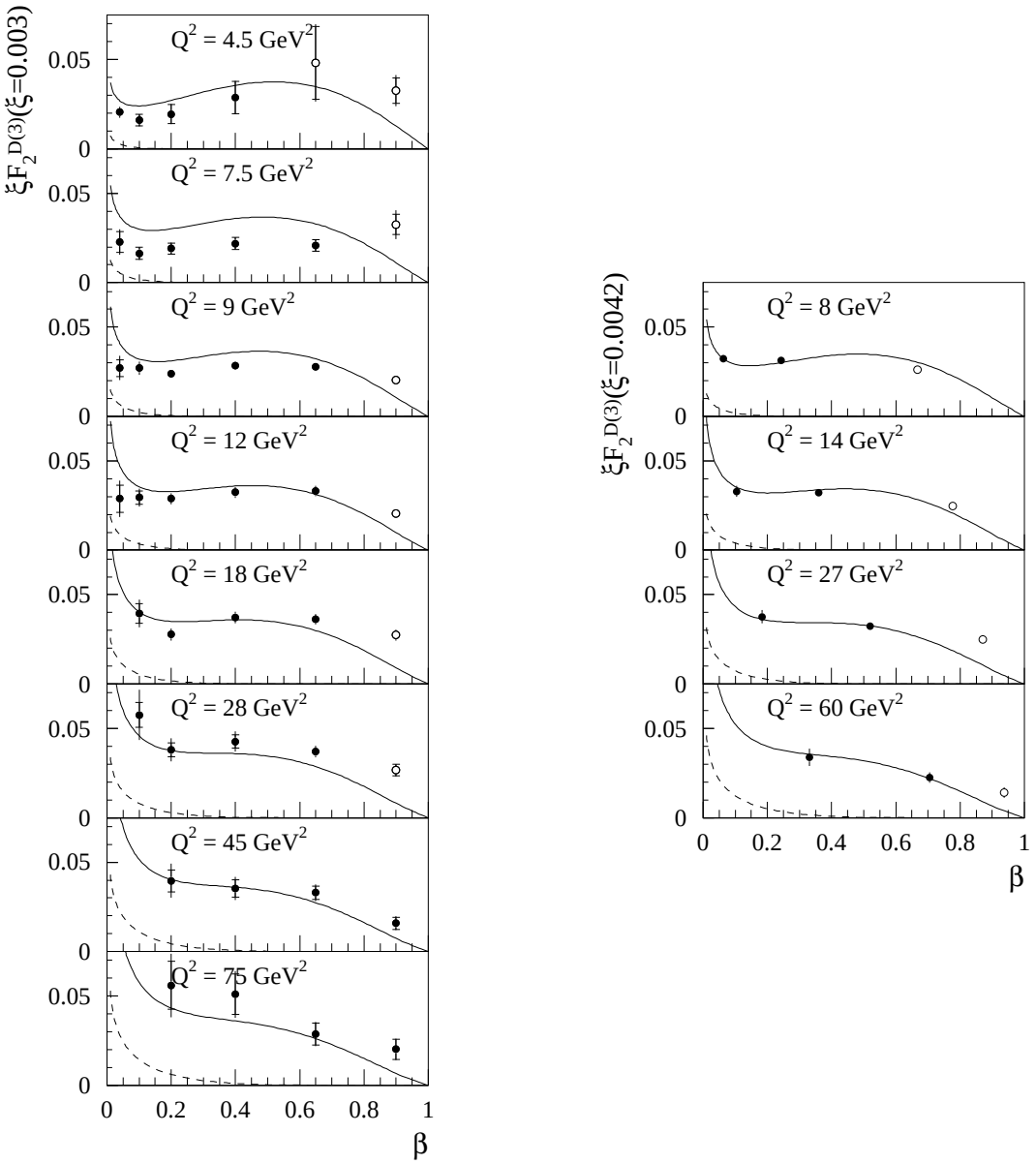

Figure 8: Dependence of the diffractive structure function $F_2^{D(3)}$ on β and Q^2, compared to data from H1 (left) and ZEUS (right) [2]. Open data points correspond to $M^2 \leq 4$ GeV^2. The charm content of the structure function is indicated as a dashed line.